HHS Public Access

Author manuscript

Immunity. Author manuscript; available in PMC 2017 February 16.

Published in final edited form as:

Immunity. 2016 February 16; 44(2): 316–329. doi:10.1016/j.immuni.2016.01.013.

Interleukin-35 limits anti-tumor immunity

Meghan E. Turnis[2,5,9], **Deepali V. Sawant**[1,2,9], **Andrea L. Szymczak-Workman**[2,7], **Lawrence P. Andrews**[1], **Greg M. Delgoffe**[2,6], **Hiroshi Yano**[1], **Amy J. Beres**[2,8], **Peter Vogel**[3], **Creg J. Workman**[1,2], and **Dario A. A. Vignali**[1,2,4,*]

[1]Department of Immunology, University of Pittsburgh, Pittsburgh, PA 15261, USA

[2]Department of Immunology, St. Jude Children's Research Hospital, Memphis, TN, 38105, USA

[3]Department of Pathology, St. Jude Children's Research Hospital, Memphis, TN, 38105, USA

[4]Tumor Microenvironment Center, University of Pittsburgh Cancer Institute, Pittsburgh, PA 15232, USA

Summary

Regulatory T (Treg) cells pose a major barrier to effective anti-tumor immunity. Although Treg cell depletion enhances tumor rejection, the ensuing autoimmune sequelae limits its utility in the clinic and highlights the need for limiting Treg cell activity within the tumor microenvironment. Interleukin-35 (IL-35) is a Treg cell-secreted cytokine that inhibits T cell proliferation and function. Using an IL-35 reporter mouse, we observed substantial enrichment of IL-35^{+} Treg cells in tumors. Neutralization with an IL-35-specific antibody or Treg cell-restricted deletion of IL-35 production limited tumor growth in multiple murine models of human cancer. Limiting intratumoral IL-35 enhanced T cell proliferation, effector function, antigen-specific responses, and long-term T cell memory. Treg cell-derived IL-35 promoted the expression of multiple inhibitory receptors (PD1, TIM3, LAG3), thereby facilitating intratumoral T cell exhaustion. These findings reveal previously unappreciated roles for IL-35 in limiting anti-tumor immunity and contributing to T cell dysfunction in the tumor microenvironment.

[*]Correspondence: dvignali@pitt.edu.
[5]Present address: Department of Hematology, St. Jude Children's Research Hospital, Memphis, TN, 38105, USA
[6]Present address: Tumor Microenvironment Center, University of Pittsburgh Cancer Institute, Pittsburgh, PA 15232, USA
[7]Present address: Department of Immunology, University of Pittsburgh, Pittsburgh, PA 15261, USA
[8]Present address: Immucor Inc., Waukesha, WI 53186, USA
[9]Co-first author

Author Contributions

MET and DVS designed and performed most of the experiments and wrote the manuscript, ALS made *Ebi3*^{Tom} reporter and *Ebi3*$^{Tom.fl/fl.Thy1.1}$ conditional reporter mice, LPA and HY helped with tumor experiments, GMD performed IP-westerns, AJB developed the micro-suppression assay, PV performed veterinary histology and analyses, CJW helped with experimental design and designed mutant mouse targeting constructs, DAAV conceived the project, directed the research, contributed to experimental design and wrote the manuscript. All authors edited and approved the manuscript.

Competing Financial Interests

The authors declare competing financial interests. DAAV and CJW have submitted patents covering IL-35 that are pending and are entitled to a share in net income generated from licensing of these patent rights for commercial development.

Introduction

Regulatory T (Treg) cells specialize in the maintenance of self-tolerance and prevention of autoimmunity (Ohkura et al., 2013; Vignali et al., 2008); however, they also restrain critical tumor-specific T cell responses. $CD4^+CD25^+$ Tregs are frequently increased in the periphery of cancer patients and specifically recruited to malignant sites, where they actively inhibit infiltrating cytotoxic T lymphocytes (CTLs) (Cao, 2010). Conversely, $CD8^+$ T cell infiltration is a positive prognostic indicator in many tumor types including breast, prostate, cervical, melanoma, and others (Galon et al., 2013; Senovilla et al., 2012). Successful anti-tumor responses require potent $CD8^+$ CTL induction and $CD4^+$ T cell help, yet the immune system is critically involved in promoting tumorigenesis by blocking anti-tumor immunity via Tregs. The ultimate goal of cancer immunotherapy is to tip the balance away from Tregs and towards tumor-specific T cell activity without causing significant adverse events, such as inflammation and autoimmune complications. To enhance cancer immunotherapy, we require a better understanding of the dominant suppressive mechanisms used by Tregs, especially those that might be selectively utilized only within the tumor microenvironment.

Treg depletion can dramatically enhance tumor rejection whilst reconstitution leads to robust tumor growth (Nishikawa and Sakaguchi, 2014). Likewise, inhibition of suppressive signaling pathways or attenuation of Treg inhibitory function has shown to decrease tumor burden and improve patient outcome (Delgoffe et al., 2013; Hodi et al., 2010; Topalian et al., 2012). Therapeutic monoclonal antibodies that target inhibitory receptor (IR) pathways (e.g. CTLA4 or PD1/PDL1) limit T-cell exhaustion, enhance $CD8^+$ T cell anti-tumoral activity and increase the ratio of activated CTL to $Foxp3^+$ Tregs in the tumor (Page et al., 2014). A role for Tregs and their secreted cytokines, IL-10 and TGFβ, in T cell exhaustion in tumors and viral infections has been suggested (Brooks et al., 2008; Ejrnaes et al., 2006; Tinoco et al., 2009). However, it remains unclear whether Tregs can directly promote exhaustion of antigen-specific T cells. Reversal of $CD8^+$ T cell exhaustion and efficient control of viral load was noted following dual blockade of Tregs and PDL1 (Penaloza-MacMaster et al., 2014) or IL-10 and PDL1 (Brooks et al., 2008). Inhibition of TGFβ signaling via expression of a dominant-negative receptor improved the functionality of exhausted $CD8^+$ T cells (Tinoco et al., 2009). Elucidation of inhibitory molecules that contribute to the suppressive tumor microenvironment, and yet exhibit a limited role in peripheral immune homeostasis, is highly desirable as it may lead to the development of effective, targeted immunotherapies with reduced adverse events.

Tregs suppress effector cells by numerous mechanisms, one of which is secretion of inhibitory cytokines (Vignali et al., 2008). IL-35, a member of the IL-12 family, is a heterodimeric inhibitory cytokine composed of the p35 subunit of IL-12 (encoded by *Il12a*) and Ebi3 (*Ebi3*) and is preferentially secreted by mouse and human Tregs (Collison et al., 2007)). IL-35 also induces the conversion of conventional T cells into a suppressive, IL-35-producing $CD4^+Foxp3^-$ induced regulatory T-cell population (iTr35 cells) (Collison et al., 2010). Multiple $IL\text{-}35^+$ cell types have been described in tumor-bearing mice and patient samples, and forced expression of IL-35 in the tumor microenvironment can drive enhanced tumor growth (Collison et al., 2007; Olson et al., 2012; Wang et al., 2013). However, the physiological impact of IL-35 on the unmanipulated tumor microenvironment has not been

examined and the mechanism by which IL-35 functions in tumors remains obscure. In this study, we tested the hypothesis that IL-35 produced by Tregs contributes substantially to the suppressive tumor milieu and that depletion will enhance tumor-specific immunity.

Results

IL-35 blockade limits tumor growth in multiple transplantable tumor models

IL-35 is produced by Tregs (Collison et al., 2007) and ~50% of $CD4^+$ T cells infiltrating primary B16 tumors are $Foxp3^+$ (Kortylewski et al., 2009). Thus, we first asked if systemic IL-35 neutralization would impact tumor growth by enhancing tumor-specific immunity. We took advantage of a unique Ebi3 monoclonal antibody (mAb) that neutralizes IL-35 but not IL-27, the other known Ebi3-containing cytokine (Collison et al., 2007). This antibody does not deplete Tregs (Figure S1A) and has an *in vivo* half-life of approximately 5 days (data not shown). Wild-type C57BL/6 mice were inoculated intradermally with B16 melanoma or subcutaneously with MC38 colon adenocarcinoma and received weekly prophylactic treatment with anti-IL-35 or IgG_{2b} isotype. Tumor growth was measured and survival monitored (Figure 1A). IL-35 neutralization significantly reduced tumor growth in both models compared to mice receiving IgG_{2b} (Figures 1B and 1C). Although survival was not improved for MC38-bearing mice, there was a significant survival advantage for anti-IL-35-treated B16-bearing mice (Figure S1B). Importantly, while the relative potency of IL-35 blockade on tumor regression was not as striking as Treg depletion using the $Foxp3^{DTR}$ system (Figures S1C and S1D), none of the anti-IL-35 treated mice exhibited inflammatory lesions following extensive histological analysis of lymph nodes, lungs, kidneys, liver, spleen, small intestine, and skin (data not shown). In contrast, the DT-treated B16 and MC38 tumor-bearing $Foxp3^{DTR}$ mice eventually succumbed to severe autoimmune inflammation around days 25–30 (Figures S1C, S1D and data not shown).

We performed additional experiments to demonstrate that this was a specific effect of IL-35 rather than IL-27. First, anti-IL-27 antibody (p28-specific) did not affect B16 growth in C57BL/6 mice compared with isotype (Figure S2A). Second, B16 growth was comparable in $Il27a^{-/-}$ (p28-deficient) mice and littermate controls, and the effect of IL-35 neutralization was identical regardless of genotype (Figure S2B).

Concurrent expression of both IL-35 subunits has been reported in some human cancers and Ebi3 is associated with lung cancer and multiple types of lymphoma (Gonin et al., 2011; Long et al., 2013; Nishino et al., 2011; Wang et al., 2013), raising the possibility that tumor-derived IL-35 limits anti-tumor immunity. However, negligible *Ebi3* and *Il12a* expression was observed in whole tumors compared with tumor-infiltrating lymphocytes (TILs) (data not shown), suggesting that IL-35 was not tumor-derived. To ensure that the anti-IL-35 treatment was not impacting tumor growth in a lymphocyte-independent manner, we implanted $Rag1^{-/-}$ mice with B16 or MC38 tumors, administered IL-35-neutralizing or control antibody prophylactically (Figure 1A). No difference in tumor growth was observed between anti-IL-35 and IgG_{2b}-treated $Rag1^{-/-}$ mice (Figure S2C).

To compare the impact of IL-35 neutralization with an established immunotherapeutic modality, we next treated B16-bearing mice with anti-PD1, which has exhibited significant

efficacy in the clinic and murine melanoma models (Page et al., 2014; Woo et al., 2012). Importantly, comparable efficacy was observed between prophylactic anti-IL-35 and anti-PD1 treatments in the B16 model (Figure 1D). We then assessed the efficacy of anti-IL-35 in a therapeutic setting alone or in combination with anti-PD1 in two distinct tumor types. Therapeutic IL-35 neutralization alone demonstrated significant efficacy while no effect was seen with anti-PD1 in B16 tumor-bearing mice (Figures 1A and 1E). In contrast, therapeutic anti-IL-35 treatment had no effect on MC38 growth compared with anti-PD1 (Figures 1F) suggesting a differential impact of these two inhibitory pathways in these two distinct tumor models. Surprisingly, the combination of anti-IL-35 and anti-PD1 did not improve efficacy in either model relative to the dominant single modalities.

We next assessed whether IL-35 neutralization could impact a metastatic tumor model by administering B16 intravenously (1.25×10^5). Mice that received prophylactic treatment with anti-IL-35 or isotype control were either monitored for survival or euthanized to determine the number of lung metastases. Anti-IL-35 recipients had significantly fewer lung metastases and enhanced survival compared to their isotype control-treated counterparts (Figures 1G and S2D). However, anti-IL-35 was unable to impact a higher dose of B16 (2.5×10^5; data not shown).

To determine whether Treg-derived IL-35 is required to constrain anti-tumor immunity, we generated mice with a Treg-restricted deletion of *Ebi3* negating their ability to produce IL-35. *Ebi3*$^{\text{Tom.L/L.Thy1.1}}$ mice harboring a floxed *Ebi3* allele and tdTomato, a bright DsRed fluorescent protein variant were crossed to *Foxp3*$^{\text{Cre-YFP}}$ (referred as *Foxp3*$^{\text{Cre-YFP}}$.*Ebi3*$^{\text{L/L}}$), which contain YFP and tdTomato-marked Tregs that do not express *Ebi3*, and thus, IL-35 (Figures S3A–3D). Mice were injected with B16 cells intradermally and tumor growth and survival monitored. Strikingly, *Foxp3*$^{\text{Cre-YFP}}$.*Ebi3*$^{\text{L/L}}$ mice had significantly smaller tumors and enhanced survival compared to *Foxp3*$^{\text{Cre-YFP}}$ controls, comparable with antibody-mediated IL-35 neutralization (Figures 1H and S2E). In addition, *Foxp3*$^{\text{Cre-YFP}}$.*Ebi3*$^{\text{L/L}}$ mice demonstrated significantly reduced number of lung metastases even when administered with a higher dose of B16 intravenously (2.5×10^5; Figure 1I).

Taken together, these data suggest that IL-35 neutralization limits tumor growth in multiple mouse models of human cancer and Treg-derived IL-35 limits immune-mediated control of tumor progression.

IL-35 limits anti-tumor immune memory in a metastatic model

Given the impact of IL-35 on anti-tumor immune responses, we questioned whether this might also impact the development of T-cell memory and responses to metastatic lesions. Mice were injected intradermally with B16, treated with anti-IL-35 or the IgG_{2b} isotype control and tumors resected after 16–18 days. Four or ten weeks following surgery, mice were re-challenged with B16 via intravenous tail vein injection and the development of metastatic lung disease monitored 3 weeks later (Figure 2A). Anti-IL-35 treated, sham-surgery mice that had not been previously exposed to tumors had significantly fewer metastases compared with their IgG_{2b}-treated counterparts (Figures 2B). Importantly, resistance to development of lung metastases was further evident in anti-IL-35 treated, tumor-resected mice (Figures 2B–2D). This was also noted following a longer intervening

period prior to re-challenge (Figure 2C). $CD8^+$ T cells infiltrating into the lungs was enhanced, with an increased proportion of activated $CD44^+CD62L^-$ cells (Figures 2E and 2F). Thus, IL-35 neutralization limits the development of melanoma lung lesions in naive mice and also enhances the long-term T cell memory response to primary tumor, limiting the development of metastatic lung disease.

IL-35 limits anti-tumor immunity in a genetically-induced tumor model

We next assessed the impact of IL-35 neutralization on a genetically-induced tumor model. We utilized the *K-ras*$^{LSL\text{-}G12D/+}$;*Trp53*$^{L/L}$ (KP) mouse, which contains an activating mutation in *K-RAS* and a loss of function mutation in p53 controlled by Cre-mediated recombination. These mutations are common in human malignancy, notably non-small cell lung cancer (NSCLC), occurring in up to 70% of cases (DuPage et al., 2009). Upon intra-tracheal (i.t.) administration of Cre recombinase, mice develop lung lesions and eventually succumb to disease within several months (Figure S4A). Thus, we inoculated KP mice i.t. with adenovirus-Cre (AdV-Cre) to induce lung tumors. Starting at week 8, tumor-bearing mice received weekly therapeutic treatment with anti-IL-35 or isotype control for ten weeks (Figure 3A). Consistent with our findings in B16-bearing mice, we observed significantly enhanced survival in the anti-IL-35 treated KP mice (Figure 3B). Histological and MRI analysis indicated significantly fewer lung lesions in AdV-Cre inoculated mice receiving IL-35 neutralizing antibody (Figures 3C–3E). However, in contrast to the transplantable tumor models, we did not observe enhanced numbers of $CD8^+$ T cells in the lungs of anti-IL-35 treated KP mice. Rather, we found significantly decreased Treg numbers and no difference in $CD8^+$ T cells (Figure 3F). These Tregs from the anti-IL-35 treated KP mice expressed significantly reduced levels of the pro-survival factor *BCL2* (Figure 3G). Importantly, despite the long-term systemic administration of IL-35 neutralizing antibody, there was no histological evidence of inflammation at sites where the tumor is reported to metastasize (mediastinal lymph nodes, liver and kidney) (Figure S4B). Thus, our data indicates that neutralization of IL-35 is effective in multiple tumor models and also demonstrates the safety and efficacy of utilizing the IL-35 neutralizing antibody in both transplantable and genetically-induced tumor models.

Increased proportion of IL-35$^+$ Tregs in the tumor microenvironment

We next investigated the source and pattern of IL-35 expression in the tumor microenvironment. We inoculated *Foxp3*$^{DTR\text{-}gfp}$ mice (used as Treg reporters; hereafter referred to as *Foxp3*^{GFP}) with B16. Quantitative RT-PCR analysis of Tregs ($CD4^+GFP^+$) and Teff ($CD4^+GFP^-$) cells revealed significantly enhanced expression of both IL-35 subunits in TIL populations compared to peripheral spleen controls (Figure 4A), consistent with previous findings (Collison et al., 2007). We next utilized a novel *Ebi3*^{Tom} reporter strain (Figures S5A and S5B) crossed to *Foxp3*$^{Cre\text{-}YFP}$ mice (used as Treg reporters) (Rubtsov et al., 2008) to facilitate analysis of *Ebi3* expression by Tregs. To demonstrate that tdTomato expression faithfully marks IL-35$^+$ Tregs, we analyzed *Ebi3* and *Il12a* gene expression in LN T cell subsets from *Foxp3*$^{Cre\text{-}YFP}$.*Ebi3*^{Tom} reporter mice. Significant upregulation of both *Ebi3* and *Il12a* transcripts were only observed in tdTomato$^+$ populations – $Ebi3^+Foxp3^+$ Tregs and $Ebi3^+Foxp3^-$ iTr35 cells (Figure S5C). Finally, to determine if Ebi3/tdTomato$^+$ T cells were secreting IL-35, peripheral lymphoid organs of

unmanipulated *Foxp3*$^{\text{Cre-YFP}}$.*Ebi3*$^{\text{Tom}}$ mice were sorted into Ebi3-Foxp3-expressing sub-populations and activated *in vitro*. Supernatants were immunoprecipitated with anti-IL12a/p35 followed by detection with anti-Ebi3 by immunoblot. IL-35 was predominantly produced by Ebi3^{+}Foxp3^{+} Tregs, and also to a lesser extent by Ebi3^{+}Foxp3^{-} iTr35 cells (Figure S5D) (Collison et al., 2010). Taken together, these data suggest that *Foxp3*$^{\text{Cre-YFP}}$.*Ebi3*$^{\text{Tom}}$ mice serve as faithful reporters for IL-35 expression by T cell subpopulations (hereafter referred to as IL-35 reporters).

Flow cytometric analysis from B16-bearing IL-35 reporter mice revealed that ~20% Tregs in the periphery (NDLN and DLN) expressed IL-35 (Figures 4B–4D), increasing dramatically in tumors, with IL-35^{+} Tregs comprising ~40% of the total Treg infiltration (Figures 4B–4D). A lower percentage of other lymphoid and myeloid cell lineages expressed *Ebi3*$^{\text{Tom}}$ (Figures S5E). iTr35 cells represented a small but consistent proportion of IL-35^{+} T cells within the peripheral CD4^{+}Foxp3^{-} T cell pool (~2–5%), with a significant increase in TILs (~5–15%; Figures 4B–4D).

To assess the suppressive capacity of this IL-35^{+} Treg sub-population, we sorted Tregs from TILs and NDLNs of B16-bearing IL-35 reporter mice based on *Foxp3*$^{\text{YFP}}$ and *Ebi3*$^{\text{Tom}}$ expression and performed *in vitro* micro-suppression assays. Ebi3^{+}Foxp3^{+} Tregs from NDLN and TILs were strongly suppressive, more so than their Ebi3^{-}Foxp3^{+} Treg counterparts (Figure 4E). We also performed concurrent micro-suppression assays with NDLN and intratumoral Tregs sorted from B16-tumor bearing *Foxp3*$^{\text{Cre-YFP}}$.*Ebi3*$^{\text{L/L}}$ mice and *Foxp3*$^{\text{Cre-YFP}}$ controls. Despite lack of a functional difference in the periphery, IL-35-deficient Tregs isolated from TILs displayed significantly reduced suppressive activity compared to their *Foxp3*$^{\text{Cre-YFP}}$ counterparts (Figure 4E).

To interrogate T-cell receptor (TCR) signaling activity in CD4^{+} T cell subpopulations, we crossed *Foxp3*$^{\text{Cre-YFP}}$.*Ebi3*$^{\text{Tom}}$ mice to the Nur77$^{\text{GFP}}$ BAC reporter mice. These mice express GFP under the control of the *Nr4a1* (Nur77) promoter, which directly correlates with the strength of TCR stimulus (Moran et al., 2011). Nur77 expression was consistently higher in Foxp3^{+} Tregs versus Foxp3^{-} Teff populations in both the DLN and TIL (Figure 4F). Ebi3^{+}Foxp3^{+} intratumoral Tregs expressed the highest level of Nur77, corresponding with their enhanced suppressive capacity observed *in vitro*.

Taken together, these data suggest that Ebi3^{+}Foxp3^{+} Tregs are the primary and dominant sources of IL-35 within the tumor microenvironment where they exhibit enhanced suppressive capacity. Thus, recruitment, induction and/or expansion of functionally competent IL-35^{+} Tregs to the tumor microenvironment may serve as another mechanism of tumor immune evasion.

IL-35 limits anti-tumor T-cell recruitment and activation

We then assessed the impact of IL-35 neutralization on T cell populations within the tumor microenvironment by flow cytometric analysis of DLN, NDLN, and TILs from anti-IL-35 and IgG_{2b}-treated B16-bearing mice. There was a significant increase in the total number of infiltrating cells, normalized for tumor volume (Figure 5A). This increase was also notable in the number, and to a lesser extent percentage, of CD4^{+}Foxp3^{-} and CD8^{+} TILs (Figures

5A–5C). The percentage and number of total Foxp3$^+$ Tregs and Ebi3$^+$Foxp3$^+$ Tregs in NDLN, DLN, and tumors remained unchanged following anti-IL-35 treatment (Figures 5A and S6A). Given that the increased accumulation of CD8$^+$ TILs relative to tumor-infiltrating Tregs is associated with more favorable prognoses in human cancers including breast, prostate, hepatocellular, and lung (Galon et al., 2013; Senovilla et al., 2012), a significant increase in the CD8:Treg ratio is also indicative of the impact of neutralizing IL-35 within the tumor microenvironment (Figure 5D).

In addition to increased numbers of infiltrating lymphocytes, intratumoral CD4$^+$ and CD8$^+$ T cells from IL-35-neutralized mice also displayed a more activated, effector memory phenotype, as determined by significantly increased percentages of CD44^{hi}CD62L^{lo} TILs (Figure 5E). IL-35 is thought to induce cell-cycle arrest at the G1–S transition (Bettini et al., 2012; Collison et al., 2007). Thus, we assessed T cell proliferation in anti-IL-35 and IgG$_{2b}$-treated, tumor-bearing mice by using Ki-67 staining and BrdU incorporation. A limited percentage of BrdU$^+$Ki-67$^+$ proliferative cells (<5%) was observed in DLN and NDLN (Figures S6B and S6C). In contrast, 15–20% BrdU$^+$Ki-67$^+$ CD8$^+$ T cells and CD4$^+$Foxp3$^+$ Tregs were observed in tumors, indicating a more rapid turnover in this inflammatory microenvironment. While the percentage of BrdU$^+$Ki-67$^+$ populations did not appear to change following anti-IL-35 treatment, there was an increase in the number of CD8$^+$ BrdU$^+$Ki-67$^+$ TILs, which was significantly enhanced within the CD44^{hi}CD62L^{lo} effector memory sub-population (Figure 5F). Thus, while IL-35 does not appear to influence the percentage of proliferating TILs, it does increase the number of intratumoral CD8$^+$ T cells in cycle, especially within the effector memory sub-population.

IL-35 limits antigen-specific anti-tumor T cell responses

We next assessed tumor antigen-specific T cell responses from IL-35-neutralized and isotype-treated B16 tumors. T cells from tumor and lymph nodes were left unstimulated, stimulated with PMA-Ionomycin (PMA-I), or stimulated with overlapping peptide pools corresponding to mouse melanoma-associated antigens (PepMix). *Ex vivo* intracellular cytokine staining of unstimulated tumor-infiltrating CD8$^+$ and CD4$^+$ T cells revealed increased cytokine expression relative to NDLN or DLN cells, a trend that was further enhanced following IL-35 neutralization (Figures 6A–6F). PMA-I stimulation revealed a slightly increased percentage of TNFα^+ CD8$^+$ and CD4$^+$ T cells and TNFα^+ IL2$^+$ CD4$^+$ T cells in the tumor DLN from anti-IL-35-treated mice (Figures 6A, 6C, 6E). Although significant changes in the responsiveness of intratumoral CD4$^+$ T cells was not observed, antigen-specific IFNγ^+/TNFα^+ CD8$^+$ CTL were significantly increased in tumors from anti-IL-35-treated mice (Figures 6B, 6D, 6F).

We further investigated the melanoma-specific response in IL-35-neutralized mice by using a TRP2$_{180\text{-}188}$ (SVYDFFVWL):MHC class I pentamer complex to detect melanoma-associated antigen specific T cells by flow cytometry. TRP2$_{180\text{-}188}$-specific CD8$^+$ TILs from anti-IL-35-treated mice were significantly enhanced compared with IgG$_{2b}$-treated mice (Figures 6G and 6H).

To assess whether T$_{reg}$-derived IL-35 limited the recruitment of antigen-specific CD8$^+$ T cells to the tumor microenvironment, we inoculated *Foxp3*$^{Cre\text{-}YFP}$.*Ebi3*$^{L/L}$ and *Foxp3*$^{Cre\text{-}YFP}$

mice with B16-OVA tumors and assessed infiltration of adoptively transferred OT-I$^{Thy1.1}$ TCR transgenic CD8$^+$ T cells to the TILs. There was also increased recruitment of transgenic Thy1.1$^+$ CD8$^+$ T cells to the TILs of a proportion of B16-OVA-bearing *Foxp3*$^{Cre\text{-}YFP}$.*Ebi3*$^{L/L}$ mice relative to *Foxp3*$^{Cre\text{-}YFP}$ controls (Figure 6I), further supporting a role for T_{reg}-derived IL-35 in limiting tumor-specific anti-tumor immune responses.

Taken together, these data highlight a previously unappreciated role for IL-35 in blunting anti-tumor immune responses by limiting expression of pro-inflammatory cytokines and generation of melanoma-specific CD8$^+$ T cell responses.

IL-35 promotes T cell exhaustion in the tumor microenvironment

Cancers and chronic infections are associated with dysfunctional CD4$^+$ and CD8$^+$ T cells with an altered differentiation program, compromised effector function and vitality (Nishikawa and Sakaguchi, 2014). The cardinal feature of these exhausted T cells is sustained and/or high intrinsic expression of multiple IRs (PD1, TIM3, LAG3, TIGIT, CD244, CD160, CTLA4) in both animal models and in humans (Blackburn et al., 2009; Kaufmann et al., 2007; Wherry et al., 2007).

Given that IL-35 blockade or Treg-restricted deletion of IL-35 mediates enhanced effector T cell responses, highlighted by increased cytokine production and proliferation, we asked if this might be due to modulated IR expression. Thus, we assessed the expression of multiple IRs (PD1, TIM3 and LAG3) on CD8$^+$ and CD4$^+$ T cells from B16-tumor bearing *Foxp3*$^{Cre\text{-}YFP}$.*Ebi3*$^{L/L}$ mice and *Foxp3*$^{Cre\text{-}YFP}$ control mice. Two distinct populations of exhausted CD8$^+$ T cells have been reported in chronic LCMV infection: cells that express high amounts of PD1 (PD1^{hi}) that are more terminally differentiated, and cells expressing intermediate levels of PD1 (PD1^{int}) that are capable of revival following PD1 blockade (Nakamoto et al., 2008; Paley et al., 2012). CD8$^+$ T cells from *Foxp3*$^{Cre\text{-}YFP}$ mice displayed high levels of PD1, TIM3 and LAG3 expression at day 14–post tumor inoculation, consistent with an exhausted profile. This CD8$^+$ T cell population was comprised primarily of cells (~40–60%) co-expressing 2 IRs (PD1^{hi}TIM3$^+$ and PD1^{hi}LAG3$^+$) or 3 IRs (PD1^{hi}TIM3$^+$LAG3$^+$), with a small percentage (~10–15%) constituting the PD1^{int} and PD1^{neg} fractions (1 and 0 IRs, respectively) (Figures 7A–7C). In contrast, CD8$^+$ T cells from the *Foxp3*$^{Cre\text{-}YFP}$.*Ebi3*$^{L/L}$ mice did not express multiple IRs, with the majority expressing low or no PD1 (PD1^{neg} and PD1^{int} fractions represented ~70–80% of total CD8$^+$ T cells; Figures 7A–7C). Similar observations were made with CD4$^+$Foxp3$^-$ T cells derived from *Foxp3*$^{Cre\text{-}YFP}$.*Ebi3*$^{L/L}$ mice (reduction from ~30% IR$^+$ cells in *Foxp3*$^{Cre\text{-}YFP}$ mice to ~10–15% IR$^+$ cells in *Foxp3*$^{Cre\text{-}YFP}$.*Ebi3*$^{L/L}$ mice; Figures 7D–7F). Consistent with these observations, we also observed a loss of IR expression on TILs in *Foxp3*$^{Cre\text{-}YFP}$.*Ebi3*$^{L/L}$ mice harboring B16 lung metastases, even though IR induction profile in the controls is less in this model (3–10% TILs in *Foxp3*$^{Cre\text{-}YFP}$ vs. 1–5% TILs in *Foxp3*$^{Cre\text{-}YFP}$.*Ebi3*$^{L/L}$ mice are PD1^{hi}, respectively; Figures S7A–S7D). Curiously, limited and inconsistent loss of IR expression was observed in mice treated with anti-IL-35, despite comparable tumor reduction and enhanced T cell activation (data not shown). It is possible that antibody-mediated IL-35 neutralization may be incomplete and that the small amount of bioactive

IL-35 that remains may induce IR expression but not limit intratumoral T cell proliferation and function, thereby leading to tumor reduction.

These results reveal an exciting new role for Treg-derived IL-35 in promoting multi-IR expression and thus shaping the exhaustion profile of T cells infiltrating the tumor microenvironment. In addition, these data offer novel insights into the mechanism of Treg-induced T cell dysfunction in chronic settings.

Discussion

Our data suggest that the presence of IL-35 in the tumor microenvironment leads to reduced lymphocytic infiltration, decreased effector cell proliferation, increased tumor burden, and decreased survival of the immunocompetent tumor-bearing host. IL-35 within the tumor dampens host memory responses, which was most notable in a metastatic lung B16 melanoma model and a genetically-induced model of lung carcinoma. Importantly, Treg-derived IL-35 shapes the exhaustion profile of tumor-infiltrating T cells by promoting multi-IR expression. Thus, IL-35 blockade provides substantial benefit in tumor clearance associated with enhanced intratumoral $CD8^+$ proliferation and/or recruitment, particularly the $CD8^+CD44^{hi}CD62L^{lo}$ population, antigen-specific inflammatory cytokine secretion and lack of exhausted T cell accumulation. Our observations demonstrate that Treg-restricted deletion of IL-35 had a comparable effect on tumor growth, suggesting that Tregs are likely to be the major, and perhaps, only meaningful source of IL-35 in the tumor microenvironment. Finally, these data suggest that IL-35 blockade may limit the suppressive environment within the tumor and thus facilitate enhanced anti-tumor immunity.

Tumors build immunosuppressive networks containing multiple negative regulatory factors, which in part involve the recruitment of Tregs and other suppressive populations. Cancer patients exhibit enhanced Treg proportions in peripheral, malignant, and tumor-associated tissues (Nishikawa and Sakaguchi, 2014). IL-35^+ Tregs appear to be preferentially enriched within the tumor microenvironment and exhibit the highest TCR signaling activity, as measured by Nur77 expression, the strongest suppressive capacity, and are a dominant source of IL-35. While it appears that Tregs are the primary source of IL-35 in the B16 tumor microenvironment, recent studies in human prostate cancer have also suggested that $CD8^+$ Tregs may utilize IL-35 as a dominant regulatory mechanism (Olson et al., 2012). Furthermore, regulatory B cells have recently been shown to produce IL-35 (Shen et al., 2014; Wang et al., 2014). Thus, the inflammatory tumor milieu may facilitate the enrichment of an IL-35^+ Treg population as one of the mechanisms for immune evasion. Whether their increased presence is due to induction of IL-35 by intratumoral Tregs, expansion, recruitment, or a combination thereof remains to be determined.

T cell exhaustion is a primary limiting factor affecting the efficacy of current cancer modalities, including CAR T cell therapies (Long et al., 2015). However, the promising anti-tumor effects noted in humans with PD1-blockade alone offers substantial potential for reversing T cell exhaustion and improving the clinical outcome of next-generation immunotherapies (Page et al., 2014). Additionally, reversal of $CD8^+$ T cell exhaustion and efficient control of viral load was noted following dual blockade of Tregs and PDL1

(Penaloza-MacMaster et al., 2014), IL-10 and PDL1 (Brooks et al., 2008) or following inhibition of TGFβ signaling (Tinoco et al., 2009). Thus, there is a clear role for Tregs and Treg-derived inhibitory cytokines in mediating T cell exhaustion, although the precise mechanisms remain to be defined. Our observation that Treg-restricted deletion of IL-35 had a dramatic effect on multi-IR expression on TILs suggests that IL-35 plays a key role in facilitating IR expression and thus perhaps exhaustion. This also supports the notion that Tregs directly contribute to T cell exhaustion. However, it remains to be determined if IL-35 directly induces IR expression or facilitates an environment in which IR expression is favored. It is also unclear whether IL-35 directly drives these events or if they occur via an intermediary. Nevertheless, our data clearly show that Treg-derived IL-35 contributes significantly to IR expression on TILs, and targeting IL-35 may limit the expression of multiple IRs, not just PD1. Lastly, our observation that the dual blockade of IL-35 and PD1 did not lead to enhanced tumor clearance supports the possibility that they might, in part, be in the same pathway. However, as IL-35 and PD1 appeared to have more dominant roles in the B16 and MC38 tumor models, respectively, they are also likely to have distinct non-overlapping roles. Indeed, while our data clearly show that Treg-derived IL-35 is required for PD1 (and other IR) expression on TIL, this need not imply that IL-35 is the only molecule that can induce PD1 or that PD1 induction is the only effect of IL-35, which may underlie the differential effects of anti-PD1 and anti-IL-35 in different tumor models.

The impact of IL-35 neutralization may vary depending on tumor model and type, and may correlate with the impact of Tregs. As Tregs appear to play a particularly dominant role in certain tumor types, it is possible that IL-35 will in turn be a more prominently utilized suppressive mechanism in cancer than other inflammatory or autoimmune diseases. Understanding these intricacies is vital for rational treatment design for cancer and other catastrophic diseases. Given the overwhelming focus on the development of multimodality approaches to the treatment of cancer, the generation of effective yet safe therapies that target intratumoral Treg function and/or stability will be paramount for the treatment of many tumor types. While our data suggest that IL-35 neutralization may represent a viable therapeutic approach, its expression within, and impact on, the human tumor microenvironment remains to be determined.

Experimental Procedures

Mice

Four to six week old C57BL/6, *Rag1*$^{-/-}$, *K-ras*$^{LSL-G12D}$, *Trp53*$^{L/L}$ and C57BL/6-Tg (TcraTcrb)1100Mjb/J OT-I mice were purchased from Jackson labs. *K-ras*$^{LSL-G12D}$ and *Trp53*$^{L/L}$ mice were crossed to obtain *K-ras*$^{LSL-G12D/+}$; *Trp53*$^{L/L}$ mice (DuPage et al., 2009). OT-I Tg mice were crossed to Foxp3$^{\text{Cre-YFP.Thy1.1}}$ mice. *Ebi3*$^{\text{Tom}}$ and *Ebi3*$^{\text{Tom.L/L.Thy1.1}}$ mice were generated in our laboratory as described in supplementary information (Figures S5 and S3). *Foxp3*$^{\text{Cre-YFP}}$ (Rubtsov et al., 2008) and *Foxp3*$^{\text{DTR-gfp}}$ (Fontenot et al., 2005) mice were obtained from A.Y. Rudensky and crossed to *Ebi3*$^{\text{Tom}}$ mice. Nur77$^{\text{GFP}}$ mice were obtained from K.A. Hogquist (Moran et al., 2011) and crossed to *Foxp3*$^{\text{Cre-YFP}}$.*Ebi3*^{Tom} mice. *Foxp3*$^{\text{DTR-gfp}}$ mice were treated with diphtheria toxin (DT) (Sigma, St. Louis, Missouri) as described (Kim et al., 2007). Mouse experiments were carried out in

AAALAC-accredited Helicobacter–, MNV–, and specific pathogen-free facilities at St. Jude Children's Research Hospital and University of Pittsburgh in accordance with IACUC guidelines.

Lymphocyte isolation and flow cytometry

Single-cell suspensions were prepared from tumors, spleens and inguinal, brachial, axillary and mediastinal lymph nodes. For isolation of TILs, solid tumors were excised after 14–18 days, tumor tissue was minced in small pieces and digested with collagenase Type IV and Dispase (both at final concentration 1mg/mL in cDMEM) for 30 minutes at 37°C. In some cases, processed tumor tissue was purified by density gradient centrifugation on 80%/40% Percoll gradient (GE Healthcare). For lung tumor experiments, lungs were perfused with PBS, minced into small pieces and digested with 1mg/ml collagenase D (Roche) for 45 minutes at 37°C. Detailed information of the staining procedures and antibody clones used for flow cytometry has been included in supplementary methods.

Tumor growth and antibody blocking experiments

B16.F10 melanoma, B16-OVA melanoma and MC38 colon adenocarcinoma models were carried out as previously described (Delgoffe et al., 2013; Turk et al., 2002; Woo et al., 2012) with some modifications detailed in supplementary methods. For antibody blocking experiments, mice were injected weekly intraperitoneally (i.p.) with 100μg anti-Ebi3 (anti-IL-35) (V1.4C4.22) or control mouse IgG_{2b} (BioXCell, West Lebanon, New Hampshire), then 50μg/week thereafter. Therapeutic B16 and MC38 experiments were conducted by injecting 1.25×10^5 B16 i.d. and 5×10^5 MC38 cells s.c. Mice received antibody treatments – anti-IL-35, anti-PD1 (clone G4) and their respective IgG_{2b} and hamster IgG isotype (BioXCell) controls once the tumors were palpable. Details regarding antibody treatments for the memory and NSCLC experiments have been provided in supplementary methods.

Real-time PCR, immunoprecipitation/western blot analysis, micro-suppression assays

RNA was extracted using TRIzol (Life Technologies) and reverse transcription performed with High Capacity Reverse Transcription kits (Applied Biosystems). Real-time PCR was performed using primers, probes, and TaqMan master mix or SYBR green chemistry (Applied Biosystems). Data were analyzed by the ΔΔCt method with housekeeping gene and calibrator sample indicated in figure legends.

For IP blots, sorted cells were expanded with PMA/Ionomycin and IL2, then activated with anti-CD3/CD28 for 72 hours or left unstimulated. Supernatants were incubated with anti–mouse IL12a (p35 clone #6, R&D Systems); IP and immunoblotting for Ebi3 was performed as described (Collison et al., 2010).

For micro-suppression assays, sorted $CD4^+Ebi3^{+/-}Foxp3^+$ Tregs derived from tumors and NDLNs were co-cultured with sorted CellTrace™ Violet, (CTV; Life Technologies) labeled $CD4^+Foxp3^-$ effector T cells (Tresponders) (4×10^3/well), along with mitomycin-C-treated TCR-β^- splenocytes (APCs) (8×10^3/well). Two-fold dilutions of Tregs were performed to obtain the various Treg/Tresponder ratios as indicated. Co-cultured cells (triplicates/

condition) were incubated for 72 hours at 37°C with soluble anti-CD3ε (1μg/mL), then analyzed by flow cytometry for CTV dilution.

Statistical analyses

To achieve reasonable power, at least 10–15 mice were used in each group, with a minimum of 3–5 mice in each group per experiment. Group means were compared with Student's t tests. Tumor growth over time was analyzed using 2way ANOVA with multiple comparisons. Event-free survival (moribund) estimates were calculated with the Kaplan–Meier method. Groups of mice were compared by log-rank test. All p values are 2-sided, and statistical significance was assessed at the 0.05 level. Analyses were conducted using GraphPad Prism software.

Supplementary Material

Refer to Web version on PubMed Central for supplementary material.

Acknowledgments

The authors wish to thank Kris Hogquist (University of Minnesota) for Nur77 mice, Merle Elloso (Janssen Research and Development) for *Il27a*$^{-/-}$ mice, and Catherine Uyttenhove and Jacques Van Snick (Ludwig Institute for Cancer Research, Brussels Branch, Brussels, Belgium) who made and provided the anti-p28 mAb. The authors also thank Mary Jo Turk (Dartmouth Medical School) for advice regarding tumor experiments, Amanda Burton for assistance in the generation of the Ebi3 conditional reporter mice, Kate Vignali for technical assistance with the targeting constructs, Christopher Calabrese and the St Jude Animal Imaging Core for assistance with MRI measurements of the KP model, Greig Lennon, Richard Cross, Parker Ingle of the St. Jude Immunology Flow Lab and Hongmei Shen, Dewayne Falkner, Aarika Yates at University of Pittsburgh flow facility for cell sorting; Abby Overacre and David Gravano for help with tumor harvests; Kristia Hamilton for lung metastasis counts; Erin Brunnazi, Amy McKenna and Karen Forbes for maintenance, breeding, and genotyping of mouse colonies; the Veterinary Pathology Core at St. Jude Children's Research Hospital for histological preparation; and the staff of the Animal Resource Center at St. Jude Children's Research Hospital and Division of Laboratory Animal Resources at University of Pittsburgh for animal husbandry and assistance. This work was supported by the National Institutes of Health (R01 AI091977 to D.A.A.V.; F32 CA168294 to M.E.T.; F32 AI098383 to G.M.D.), NCI Comprehensive Cancer Center Support CORE grant (CA21765, to D.A.A.V.), and ALSAC (to D.A.A.V.)

References

Bettini M, Castellaw AH, Lennon GP, Burton AR, Vignali DA. Prevention of autoimmune diabetes by ectopic pancreatic beta-cell expression of interleukin-35. Diabetes. 2012; 61:1519–1526. [PubMed: 22427377]

Blackburn SD, Shin H, Haining WN, Zou T, Workman CJ, Polley A, Betts MR, Freeman GJ, Vignali DA, Wherry EJ. Coregulation of CD8+ T cell exhaustion by multiple inhibitory receptors during chronic viral infection. Nat Immunol. 2009; 10:29–37. [PubMed: 19043418]

Brooks DG, Ha SJ, Elsaesser H, Sharpe AH, Freeman GJ, Oldstone MB. IL-10 and PD-L1 operate through distinct pathways to suppress T-cell activity during persistent viral infection. Proceedings of the National Academy of Sciences of the United States of America. 2008; 105:20428–20433. [PubMed: 19075244]

Cao X. Regulatory T cells and immune tolerance to tumors. Immunol Res. 2010; 46:79–93. [PubMed: 19763889]

Collison LW, Chaturvedi V, Henderson AL, Giacomin PR, Guy C, Bankoti J, Finkelstein D, Forbes K, Workman CJ, Brown SA, et al. IL-35-mediated induction of a potent regulatory T cell population. Nat Immunol. 2010; 11:1093–1101. [PubMed: 20953201]

Collison LW, Workman CJ, Kuo TT, Boyd K, Wang Y, Vignali KM, Cross R, Sehy D, Blumberg RS, Vignali DA. The inhibitory cytokine IL-35 contributes to regulatory T-cell function. Nature. 2007; 450:566–569. [PubMed: 18033300]

Delgoffe GM, Woo SR, Turnis ME, Gravano DM, Guy C, Overacre AE, Bettini ML, Vogel P, Finkelstein D, Bonnevier J, et al. Stability and function of regulatory T cells is maintained by a neuropilin-1-semaphorin-4a axis. Nature. 2013; 501:252–256. [PubMed: 23913274]

DuPage M, Dooley AL, Jacks T. Conditional mouse lung cancer models using adenoviral or lentiviral delivery of Cre recombinase. Nature protocols. 2009; 4:1064–1072. [PubMed: 19561589]

Ejrnaes M, Filippi CM, Martinic MM, Ling EM, Togher LM, Crotty S, von Herrath MG. Resolution of a chronic viral infection after interleukin-10 receptor blockade. J Exp Med. 2006; 203:2461–2472. [PubMed: 17030951]

Fontenot JD, Rasmussen JP, Williams LM, Dooley JL, Farr AG, Rudensky AY. Regulatory T cell lineage specification by the forkhead transcription factor foxp3. Immunity. 2005; 22:329–341. [PubMed: 15780990]

Galon J, Mlecnik B, Bindea G, Angell HK, Berger A, Lagorce C, Lugli A, Zlobec I, Hartmann A, Bifulco C, et al. Towards the introduction of the 'Immunoscore' in the classification of malignant tumours. J Pathol. 2013; 232:199–209. [PubMed: 24122236]

Gonin J, Larousserie F, Bastard C, Picquenot JM, Couturier J, Radford-Weiss I, Dietrich C, Brousse N, Vacher-Lavenu MC, Devergne O. Epstein-Barr virus-induced gene 3 (EBI3): a novel diagnosis marker in Burkitt lymphoma and diffuse large B-cell lymphoma. PLoS One. 2011; 6:e24617. [PubMed: 21931777]

Hodi FS, O'Day SJ, McDermott DF, Weber RW, Sosman JA, Haanen JB, Gonzalez R, Robert C, Schadendorf D, Hassel JC, et al. Improved survival with ipilimumab in patients with metastatic melanoma. N Engl J Med. 2010; 363:711–723. [PubMed: 20525992]

Kaufmann DE, Kavanagh DG, Pereyra F, Zaunders JJ, Mackey EW, Miura T, Palmer S, Brockman M, Rathod A, Piechocka-Trocha A, et al. Upregulation of CTLA-4 by HIV-specific CD4+ T cells correlates with disease progression and defines a reversible immune dysfunction. Nat Immunol. 2007; 8:1246–1254. [PubMed: 17906628]

Kim JM, Rasmussen JP, Rudensky AY. Regulatory T cells prevent catastrophic autoimmunity throughout the lifespan of mice. Nat Immunol. 2007; 8:191–197. [PubMed: 17136045]

Kortylewski M, Xin H, Kujawski M, Lee H, Liu Y, Harris T, Drake C, Pardoll D, Yu H. Regulation of the IL-23 and IL-12 balance by Stat3 signaling in the tumor microenvironment. Cancer Cell. 2009; 15:114–123. [PubMed: 19185846]

Long AH, Haso WM, Shern JF, Wanhainen KM, Murgai M, Ingaramo M, Smith JP, Walker AJ, Kohler ME, Venkateshwara VR, et al. 4–1BB costimulation ameliorates T cell exhaustion induced by tonic signaling of chimeric antigen receptors. Nat Med. 2015; 21:581–590. [PubMed: 25939063]

Long J, Zhang X, Wen M, Kong Q, Lv Z, An Y, Wei XQ. IL-35 over-expression increases apoptosis sensitivity and suppresses cell growth in human cancer cells. Biochem Biophys Res Commun. 2013; 430:364–369. [PubMed: 23154182]

Moran AE, Holzapfel KL, Xing Y, Cunningham NR, Maltzman JS, Punt J, Hogquist KA. T cell receptor signal strength in Treg and iNKT cell development demonstrated by a novel fluorescent reporter mouse. J Exp Med. 2011; 208:1279–1289. [PubMed: 21606508]

Nakamoto N, Kaplan DE, Coleclough J, Li Y, Valiga ME, Kaminski M, Shaked A, Olthoff K, Gostick E, Price DA, et al. Functional restoration of HCV-specific CD8 T cells by PD-1 blockade is defined by PD-1 expression and compartmentalization. Gastroenterology. 2008; 134:1927–1937. 1937 e1921–1922. [PubMed: 18549878]

Nishikawa H, Sakaguchi S. Regulatory T cells in cancer immunotherapy. Current opinion in immunology. 2014; 27:1–7. [PubMed: 24413387]

Nishino R, Takano A, Oshita H, Ishikawa N, Akiyama H, Ito H, Nakayama H, Miyagi Y, Tsuchiya E, Kohno N, et al. Identification of Epstein-Barr virus-induced gene 3 as a novel serum and tissue biomarker and a therapeutic target for lung cancer. Clin Cancer Res. 2011; 17:6272–6286. [PubMed: 21849417]

Ohkura N, Kitagawa Y, Sakaguchi S. Development and maintenance of regulatory T cells. Immunity. 2013; 38:414–423. [PubMed: 23521883]

Olson BM, Jankowska-Gan E, Becker JT, Vignali DA, Burlingham WJ, McNeel DG. Human prostate tumor antigen-specific CD8+ regulatory T cells are inhibited by CTLA-4 or IL-35 blockade. J Immunol. 2012; 189:5590–5601. [PubMed: 23152566]

Page DB, Postow MA, Callahan MK, Allison JP, Wolchok JD. Immune modulation in cancer with antibodies. Annu Rev Med. 2014; 65:185–202. [PubMed: 24188664]

Paley MA, Kroy DC, Odorizzi PM, Johnnidis JB, Dolfi DV, Barnett BE, Bikoff EK, Robertson EJ, Lauer GM, Reiner SL, Wherry EJ. Progenitor and terminal subsets of CD8+ T cells cooperate to contain chronic viral infection. Science. 2012; 338:1220–1225. [PubMed: 23197535]

Penaloza-MacMaster P, Kamphorst AO, Wieland A, Araki K, Iyer SS, West EE, O'Mara L, Yang S, Konieczny BT, Sharpe AH, et al. Interplay between regulatory T cells and PD-1 in modulating T cell exhaustion and viral control during chronic LCMV infection. J Exp Med. 2014; 211:1905–1918. [PubMed: 25113973]

Rubtsov YP, Rasmussen JP, Chi EY, Fontenot J, Castelli L, Ye X, Treuting P, Siewe L, Roers A, Henderson WR Jr, et al. Regulatory T cell-derived interleukin-10 limits inflammation at environmental interfaces. Immunity. 2008; 28:546–558. [PubMed: 18387831]

Senovilla L, Vacchelli E, Galon J, Adjemian S, Eggermont A, Fridman WH, Sautes-Fridman C, Ma Y, Tartour E, Zitvogel L, et al. Trial watch: Prognostic and predictive value of the immune infiltrate in cancer. Oncoimmunology. 2012; 1:1323–1343. [PubMed: 23243596]

Shen P, Roch T, Lampropoulou V, O'Connor RA, Stervbo U, Hilgenberg E, Ries S, Dang VD, Jaimes Y, Daridon C, et al. IL-35-producing B cells are critical regulators of immunity during autoimmune and infectious diseases. Nature. 2014

Tinoco R, Alcalde V, Yang Y, Sauer K, Zuniga EI. Cell-intrinsic transforming growth factor-beta signaling mediates virus-specific CD8+ T cell deletion and viral persistence in vivo. Immunity. 2009; 31:145–157. [PubMed: 19604493]

Topalian SL, Hodi FS, Brahmer JR, Gettinger SN, Smith DC, McDermott DF, Powderly JD, Carvajal RD, Sosman JA, Atkins MB, et al. Safety, activity, and immune correlates of anti-PD-1 antibody in cancer. N Engl J Med. 2012; 366:2443–2454. [PubMed: 22658127]

Turk MJ, Wolchok JD, Guevara-Patino JA, Goldberg SM, Houghton AN. Multiple pathways to tumor immunity and concomitant autoimmunity. Immunol Rev. 2002; 188:122–135. [PubMed: 12445286]

Vignali DA, Collison LW, Workman CJ. How regulatory T cells work. Nat Rev Immunol. 2008; 8:523–532. [PubMed: 18566595]

Wang RX, Yu CR, Dambuza IM, Mahdi RM, Dolinska MB, Sergeev YV, Wingfield PT, Kim SH, Egwuagu CE. Interleukin-35 induces regulatory B cells that suppress autoimmune disease. Nat Med. 2014; 20:633–641. [PubMed: 24743305]

Wang Z, Liu JQ, Liu Z, Shen R, Zhang G, Xu J, Basu S, Feng Y, Bai XF. Tumor-Derived IL-35 Promotes Tumor Growth by Enhancing Myeloid Cell Accumulation and Angiogenesis. J Immunol. 2013; 190:2415–2423. [PubMed: 23345334]

Wherry EJ, Ha SJ, Kaech SM, Haining WN, Sarkar S, Kalia V, Subramaniam S, Blattman JN, Barber DL, Ahmed R. Molecular signature of CD8+ T cell exhaustion during chronic viral infection. Immunity. 2007; 27:670–684. [PubMed: 17950003]

Woo SR, Turnis ME, Goldberg MV, Bankoti J, Selby M, Nirschl CJ, Bettini ML, Gravano DM, Vogel P, Liu CL, et al. Immune inhibitory molecules LAG-3 and PD-1 synergistically regulate T-cell function to promote tumoral immune escape. Cancer Res. 2012; 72:917–927. [PubMed: 22186141]

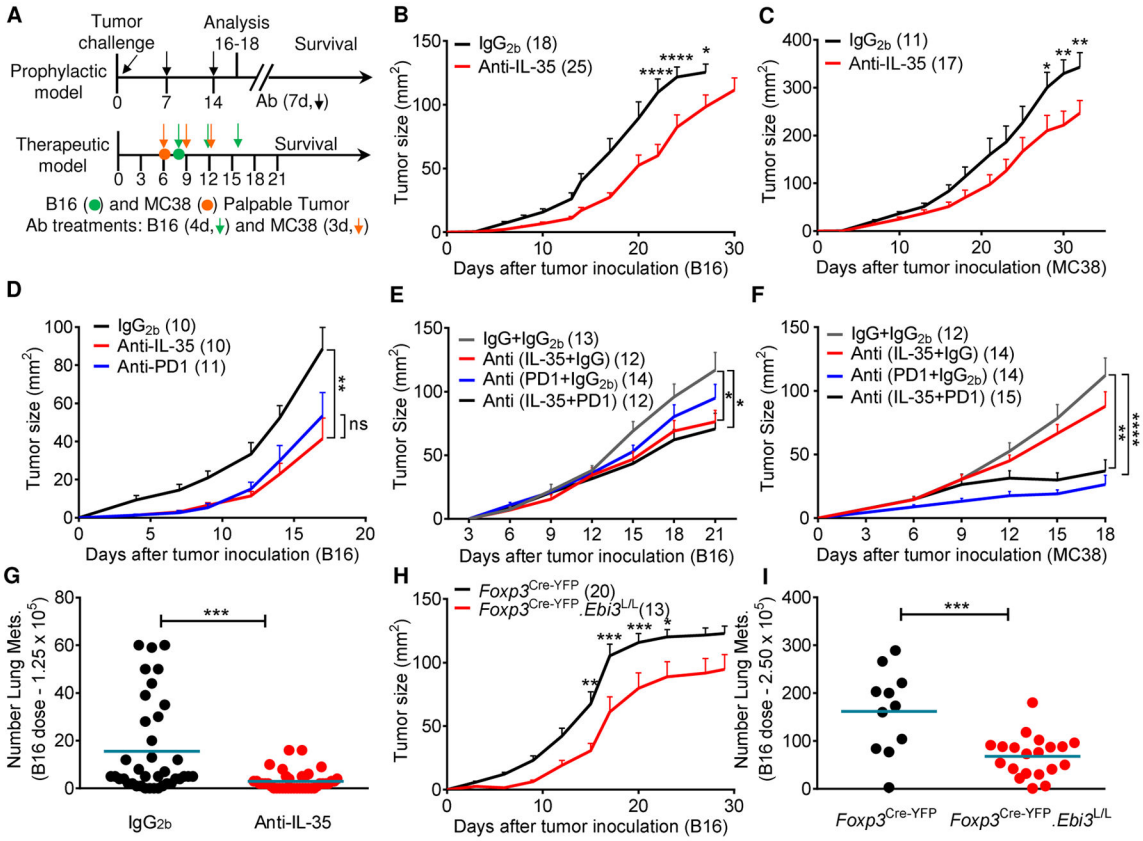

Fig 1. IL-35 blockade reduces tumor burden in multiple transplantable tumor models

(A) Schematic of transplantable tumor models (Prophylactic and Therapeutic) and timeline for antibody dosage. Mice were injected on day 0 with tumor cells (1.25×10^5 B16 i.d. or 5×10^5 MC38 s.c.). In the prophylactic model, mice received weekly administration of anti-IL-35 or IgG_{2b} antibody (Ab) where indicated (100 μg first dose, 50 μg additional doses) (Figures 1B–D, 1G). For therapeutic analysis (Figures 1E and 1F), mice received antibody treatments at the indicated time-points once the tumor became palpable. (B) Tumor growth curves of C57BL/6 mice injected i.d. with B16 plus weekly antibody administration as in part (A). (C) Tumor growth curves of C57BL/6 mice injected s.c. with MC38 plus weekly antibody administration as in part (A). (D) Tumor growth curves of C57BL/6 mice injected i.d. with B16 on day 0 plus weekly antibody administration (anti-IL-35, anti-PD1, or IgG_{2b}) as in part (A). (E) Tumor growth curves of C57BL/6 mice injected i.d. with B16 on day 0 followed by anti-IL-35/anti-PD1 or matched IgG controls every four days once the tumors were palpable (days 8, 12 and 16). (F) Tumor growth curves of C57BL/6 mice injected s.c. with MC38 on day 0 followed by anti-IL-35/anti-PD1 or matched IgG controls every three days once the tumors were palpable (days 6, 9 and 12). (G) C57BL/6 mice were injected i.v. with a low dose of B16 (1.25×10^5) on day 0 along with weekly antibody administration as in part (A). Mice were euthanized on day 21 and lung metastases were counted by microscopy. (H) Tumor growth curves of *Foxp3*$^{\text{Cre-YFP}}$.*Ebi3*$^{\text{L/L}}$ and *Foxp3*$^{\text{Cre-YFP}}$ control mice injected i.d. with B16. (I) Lung metastases counts in *Foxp3*$^{\text{Cre-YFP}}$.*Ebi3*$^{\text{L/L}}$ and *Foxp3*$^{\text{Cre-YFP}}$ control mice injected i.v. with a higher dose of B16 (2.5×10^5), assessed day 14 post-injection. Data

represent 3–4 independent experiments (6 for panel 1G) with total number of mice per group in parentheses. Error bars represent SEM; *, $p < 0.05$; **, $p < 0.01$; ***, $p < 0.001$; ****, $p < 0.0001$; ns, non-significant as determined by 2way ANOVA with multiple comparisons (panels 1B, 1C, 1D, 1E, 1F, 1H) or Unpaired Student's t-test (panels 1G and 1I). See also Figures S1, S2 and S3.

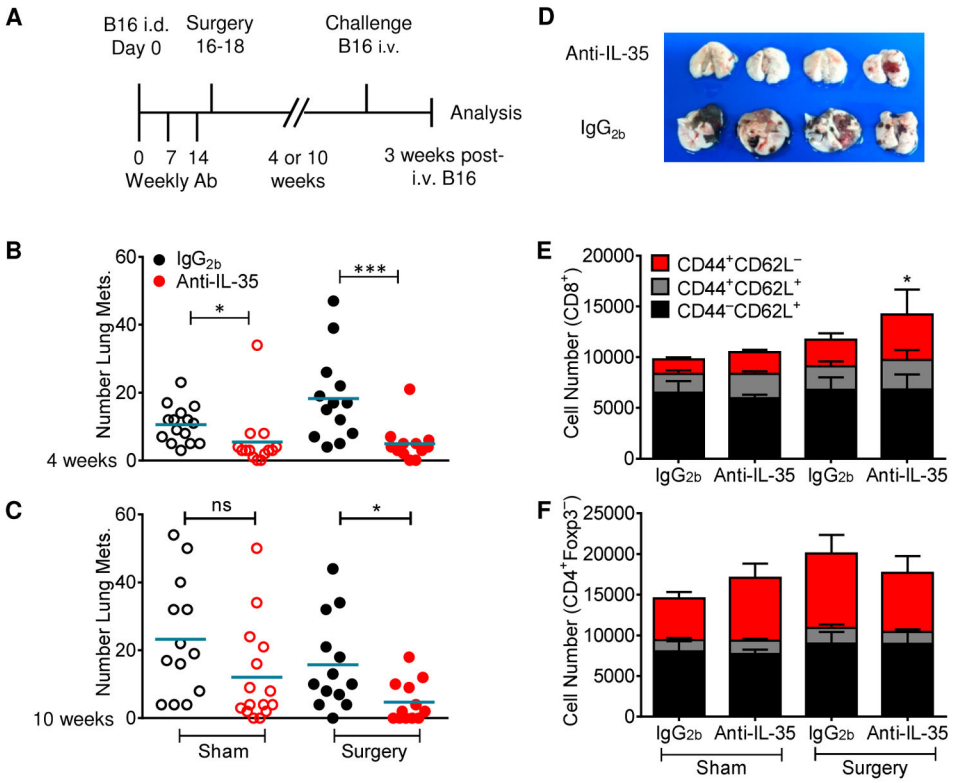

Fig 2. Neutralization of IL-35 enhances anti-tumor immune memory

(A) Diagram of treatment, surgery, and re-challenge strategy. C57BL/6 mice were injected i.d. with B16 on day 0. Anti-IL-35 or IgG_{2b} was administered weekly on days 0, 7, and 14 (100μg, 50μg, 50μg). Tumors were surgically resected on day 16–18. (B,C) Mice were re-challenged with B16 i.v. 4 (B) or 10 (C) weeks following surgery. Three weeks after re-challenge, lung metastases were counted by microscopy. (D) Photograph of lungs from 4–week re-challenged mice. (E,F) Cumulative CD44/CD62L staining from lungs of 4–week re-challenged mice, gated on $CD8^+$ (E) or $CD4^+Foxp3^-$ (F) T cells. Data represent 3–4 independent experiments; Error bars represent SEM; *, $p < 0.05$; ***, $p < 0.001$; ns, non-significant (Unpaired Student's t-test).

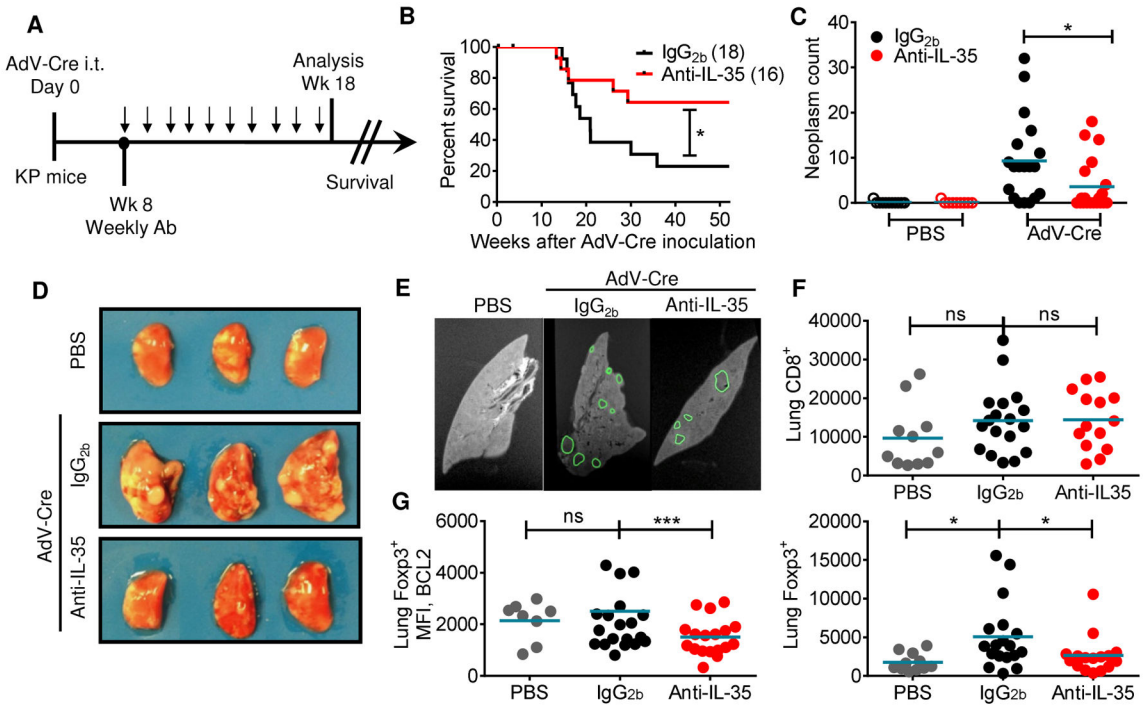

Fig 3. Neutralization of IL-35 enhances anti-tumor immunity in a genetically-induced tumor model

(A) Schematic of the *K-ras*$^{LSL\text{-}G12D/+}$;*Trp53*$^{L/L}$ (KP) mouse model. Mice were inoculated i.t. with 2.5×10^7 IU AdV-Cre, then injected therapeutically with ten weekly doses of anti-IL-35 or IgG$_{2b}$ isotype control (100μg/week) starting at week eight. (B) Cumulative survival curve of AdV-Cre inoculated, antibody-treated mice. (C-G) Following antibody treatments, lungs and lymph nodes were harvested at 18 weeks. (C) Quantification of lung lesions by MRI in control (PBS) and induced (AdV-Cre) mice treated with anti-IL-35 or IgG$_{2b}$ antibodies. (D) Representative picture of lung lobes from each treatment group. (E) Representative MRI slice from each treatment group with outline of ROIs, used to quantify lesion number and volume, shown in green. (F) Flow cytometric analysis of lung tissue indicating number of CD8$^+$ T cells (top) and CD4$^+$Foxp3$^+$ Tregs (bottom) for the various treatment groups (PBS, IgG$_{2b}$ and anti-IL-35). (G) Flow cytometric analysis of lung tissue indicating MFI of BCL2 on Tregs (bottom) for the various treatment groups (PBS, IgG$_{2b}$ and anti-IL-35). Data represent 3 independent experiments. Survival curves were analyzed for statistical significance by log-rank test. Error bars represent SEM; *, $p < 0.05$; ***, $p < 0.001$; ns, non-significant as determined by Unpaired Student's t-test (panel C) and 1 way ANOVA (panels F and G). See also Figure S4.

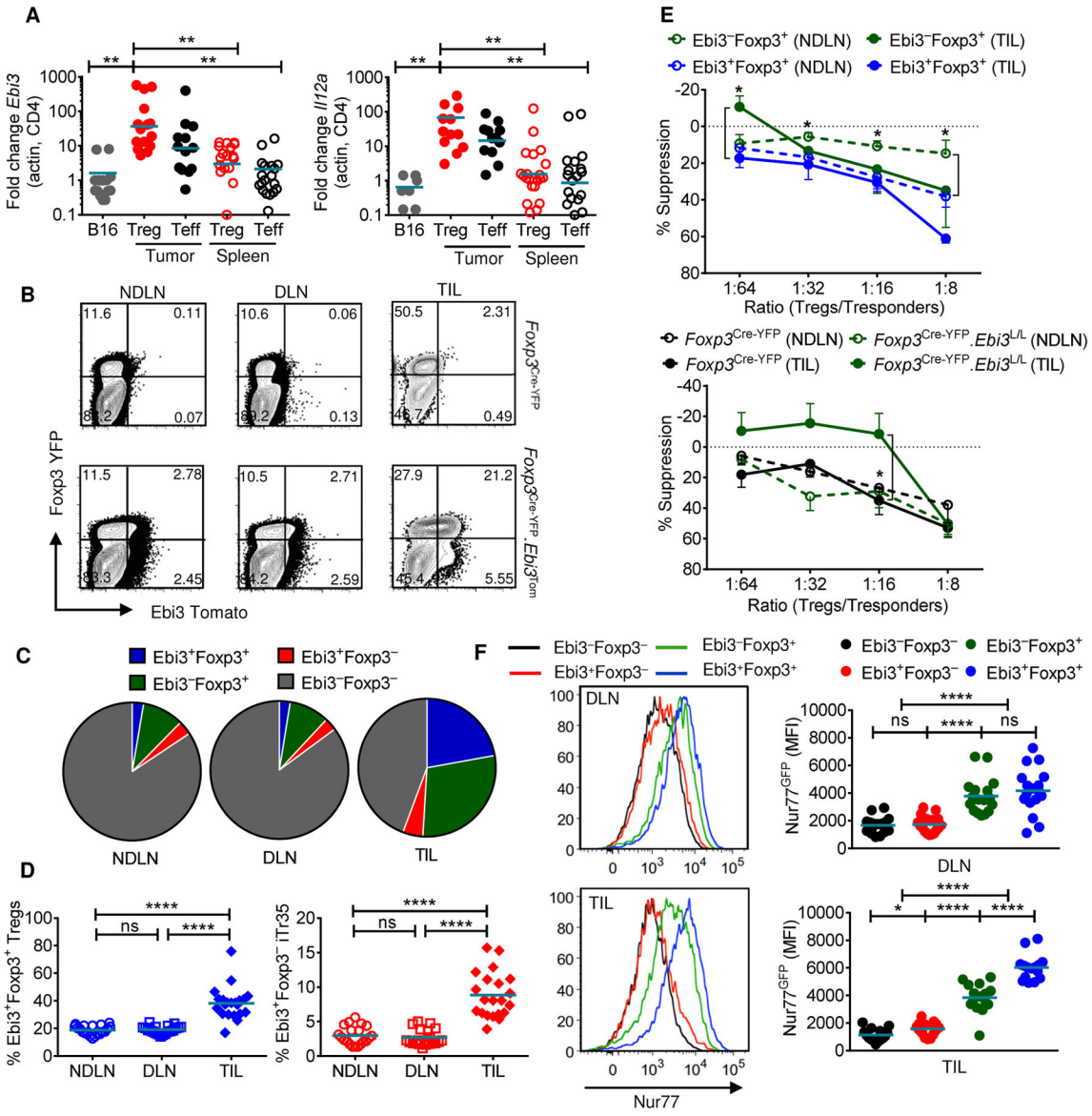

Fig 4. Increased percentages of functionally superior IL-35-expressing Tregs in TILs

(A) Tumors and spleens were harvested from day 16–18 B16-bearing *Foxp3*^{GFP} mice and sorted for Treg (CD4$^+$GFP$^+$) and T$_{eff}$ (CD4$^+$GFP$^-$) cells. Quantitative RT-PCR analysis of IL-35 subunits *Il12a* and *Ebi3*, with β-*actin* used as endogenous control. Controls are whole B16 cDNA isolated from *Rag1*$^{-/-}$ B16-bearing mice. (B) Representative flow cytometric plots of NDLN, DLN, and TILs from B16-bearing *Foxp3*$^{Cre\text{-}YFP}$ or *Foxp3*$^{Cre\text{-}YFP}$.*Ebi3*^{Tom} (IL-35 reporter) mice, gated on CD4$^+$ T cells. (C) Pie charts representing percentages of Ebi3$^+$ and Ebi3$^-$ Foxp3$^+$ Tregs and Foxp3$^-$ Teffs in NDLN, DLN and TILs of B16-bearing IL-35 reporter mice, gated on CD4$^+$ T cells. (D) Scatter plots representing percentages of Ebi3$^+$Foxp3$^+$ Tregs in the total Treg compartment (gated on CD4$^+$Foxp3$^+$ T cells) (left) and Ebi3$^+$Foxp3$^-$ iTr35 cells in the total Teff compartment (gated on CD4$^+$Foxp3$^-$ T cells) at NDLN, DLN and TIL. (E) Micro-suppression assays using sorted Ebi3$^+$Foxp3$^+$ and Ebi3$^-$Foxp3$^+$ Tregs from NDLN (open circles) and TIL (closed circles) of B16 tumor-

bearing mice (Top). Micro-suppression assays using sorted *Foxp3*$^{Cre\text{-}YFP}$ and *Foxp3*$^{Cre\text{-}YFP}$*Ebi3*$^{L/L}$ Tregs from NDLN (open circles) and TIL (closed circles) of B16 tumor-bearing mice (Bottom). For both experiments, CD4^{+}Foxp3^{-} splenocytes were used as responders (Tresponders). Plots represent percent suppression at the indicated Treg/Tresponder ratios; representative experiment of 3–4 independent replicates shown. (F) MFI of Nur77^{GFP} gated on CD4^{+} T cells; Foxp3/Ebi3-expressing Tregs and Teff sub-populations from *Foxp3*$^{Cre\text{-}YFP}$.*Ebi3*^{Tom} x Nur77^{GFP} BAC reporter mice with representative histograms shown, DLN, top; TIL, bottom. Data represent 3–4 independent experiments; Error bars represent SEM; *, $p < 0.05$; **, $p < 0.01$; ****, $p < 0.0001$ ns, non-significant (Unpaired Student's t-test). See also Figure S5.

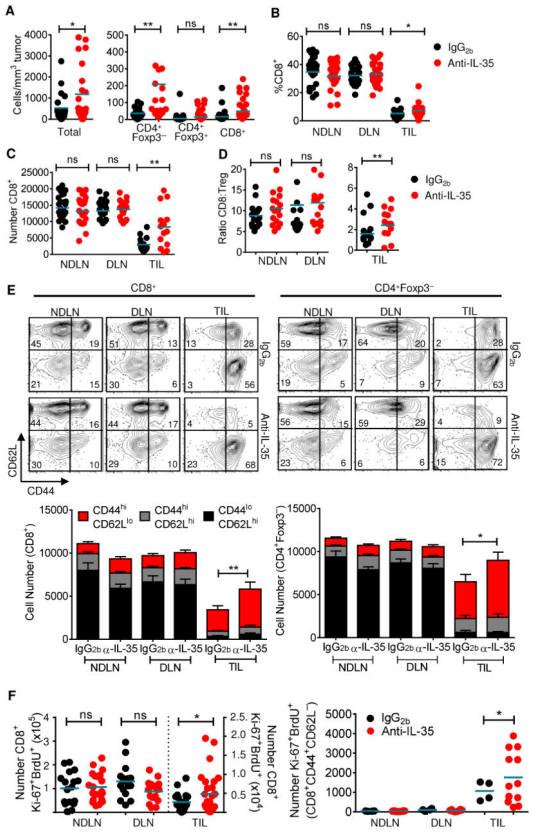

Fig 5. Increased infiltration and activation in the TILs of IL-35-neutralized mice

Tissues were harvested at day 16–18 from B16-bearing mice treated prophylactically with IgG_{2b}− or anti-IL-35 and analyzed by flow cytometry. (A) Representative scatter dot plots representing absolute number of infiltrating lymphocytes (left) or T cell subsets (right) per mm^3 tumor mass from IgG_{2b}− or anti-IL-35–treated B16-bearing mice. (B and C) Percentage and absolute number of $CD8^+$ T cells in NDLN, DLN, and TILs of IgG_{2b}− or anti-IL-35–treated B16-bearing mice. (D) Ratio of $CD8^+$ T cells to $Foxp3^+$ Tregs in NDLN, DLN, and TILs of IgG_{2b}− or anti-IL-35-treated B16-bearing mice. (E) Cumulative CD44/CD62L staining in indicated organs, gated on $CD8^+$ (left) or $CD4^+Foxp3^-$ (right) with representative flow cytometric plots shown above. (F) 18 hours prior to harvest, B16-bearing, IgG_{2b} − or anti-IL-35–treated C57BL/6 mice were injected with BrdU. Absolute number of $BrdU^+Ki\text{-}67^+$ cells (gated on $CD8^+$) in indicated tissues (left). Absolute number of $BrdU^+Ki\text{-}67^+$ cells (gated on $CD8^+CD44^{hi}CD62L^{lo}$) in indicated tissues (right). Data represent 3 independent experiments. Error bars represent SEM; *, $p < 0.05$; **, $p < 0.01$; ns, non-significant (1way ANOVA). See also Figure S6.

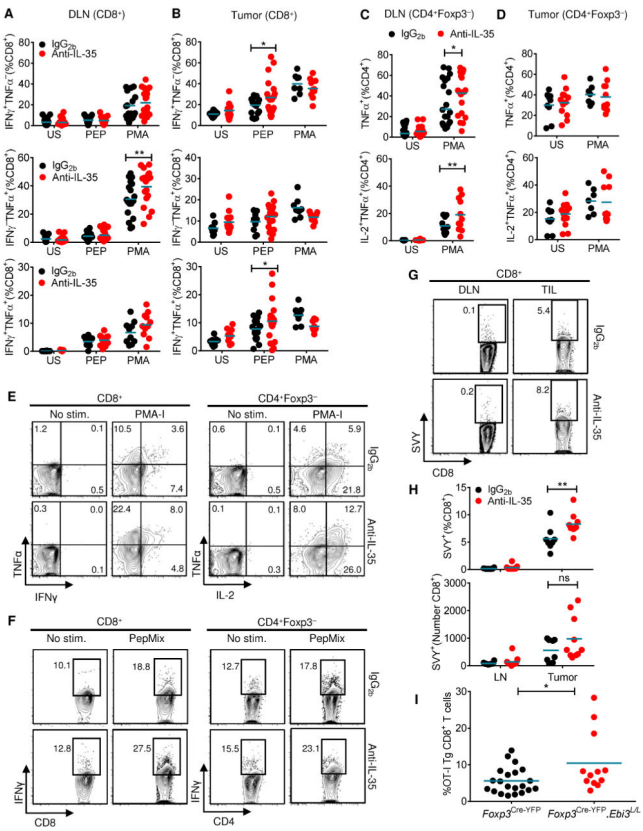

Fig 6. Enhanced cytokine production in tumor-associated tissues of IL-35-neutralized animals

Tissues were harvested at day 16–18 from B16-bearing mice treated prophylactically with IgG_{2b-} or anti-IL-35 and analyzed by intracellular staining under the following conditions: unstimulated, stimulated with PMA-Ionomycin (PMA-I) or stimulated with PepMix. (A,B) Scatter plots depicting percentage of $IFN\gamma^+$, $TNF\alpha^+$ and $IFN\gamma^+TNF\alpha^+$ $CD8^+$ T cells from DLN and TIL. (C,D) Scatter plots depicting percentage of $TNF\alpha^+$ and $TNF\alpha^+IL2^+$ $CD4^+Foxp3^-$T cells from DLN and TIL. (E) Representative flow cytometric plots of polyfunctional DLN, stimulated as indicated. Numbers represent percent positive of parent population in each quadrant. (F) Representative flow cytometric plots of IFNγ expression from TIL, stimulated as indicated. Numbers represent percent positive of parent population. (G) H2-K^b–restricted $TRP2_{180\text{-}188}$ pentamer ("SVY") analysis of freshly isolated tissues from IgG_{2b-} or anti-IL-35–treated tumor-bearing mice, numbers represent percent positive of $CD8^+$ T cells. (H) Percent and absolute numbers of H2-K^b–restricted $TRP2_{180\text{-}188}$ pentamer-positive $CD8^+$ cells from DLN and TILs of IgG_{2b}- or anti-IL-35-treated tumor-bearing mice. (I) B16-OVA tumor-bearing *Foxp3*$^{Cre\text{-}YFP}$.*Ebi3*$^{L/L}$ and *Foxp3*$^{Cre\text{-}YFP}$ mice received 5×10^6 TCR transgenic (Tg) OT-I $Thy1.1^+$ $CD8^+$ T cells i.v. once palpable tumors developed (day 10–12). Scatter plot depicting percent infiltration of OT-I $Thy1.1^+$ Tg $CD8^+$ T cells 4-days post adoptive transfer into tumors of recipient mice assessed by flow analysis. Data represent 3–4 independent experiments; Error bars represent SEM; *, $p < 0.05$; **, $p < 0.01$; ns, non-significant (1way ANOVA for panels A-D and H, Unpaired Student's t-test for panel I).

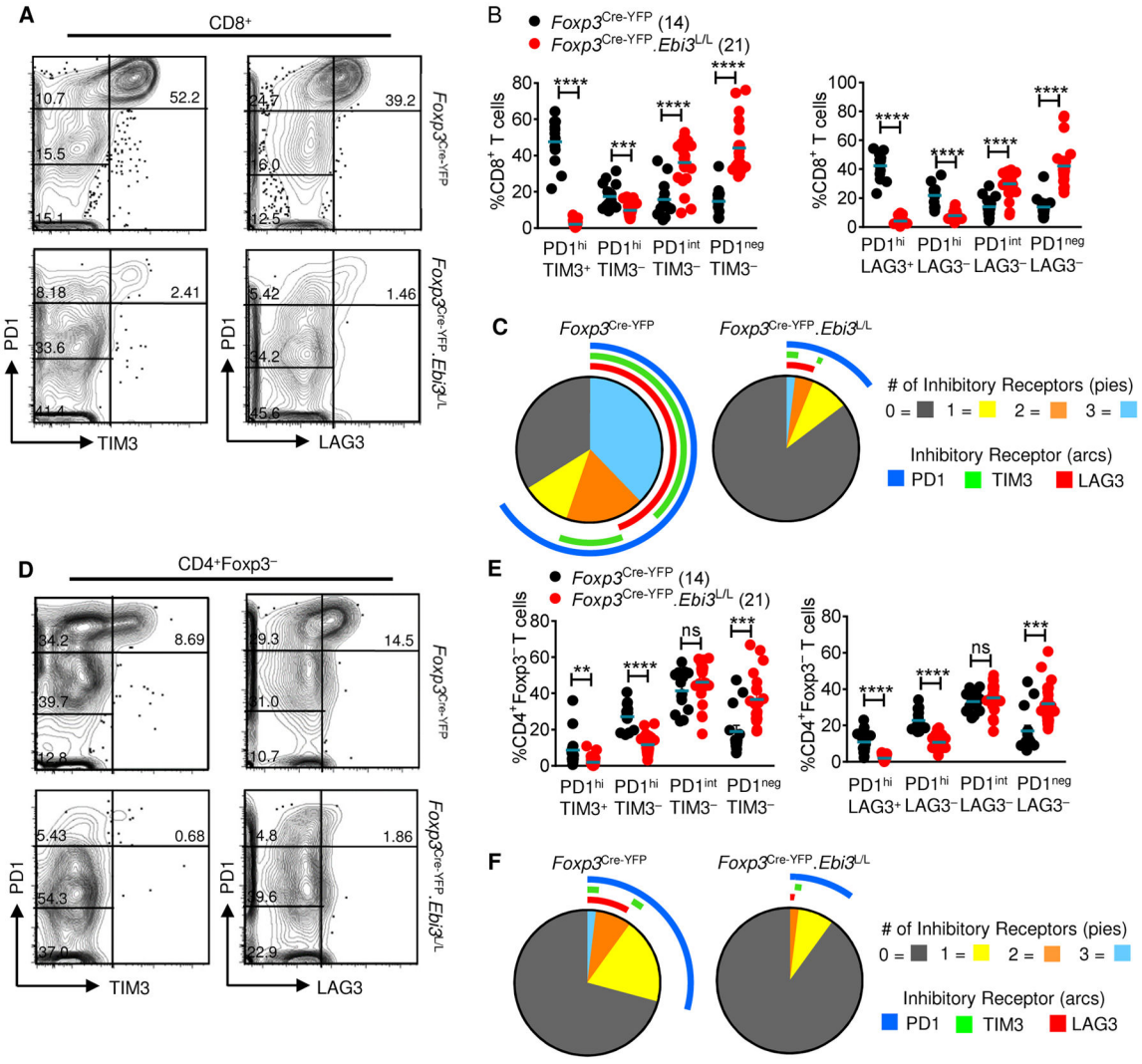

Fig 7. Treg-specific IL-35 deletion results in loss of exhausted T cells in the tumor microenvironment

Tissues were harvested at day 14 from B16-bearing *Foxp3*$^{\text{Cre-YFP}}$.*Ebi3*$^{\text{L/L}}$ and *Foxp3*$^{\text{Cre-YFP}}$ control mice and analyzed by flow cytometry. (A) Flow cytometric analysis depicting expression of inhibitory receptors (PD1/TIM3 and PD1/LAG3) on tumor-infiltrating CD8^{+} T cells from B16 tumor-bearing *Foxp3*$^{\text{Cre-YFP}}$.*Ebi3*$^{\text{L/L}}$ and *Foxp3*$^{\text{Cre-YFP}}$ control mice. Cells gated on CD8^{+} T cells, and assessed for percentage of PD1-high (PD1$^{\text{hi}}$), PD1-intermediate (PD1$^{\text{int}}$) and PD1-negative (PD1$^{\text{neg}}$) fractions co-expressing TIM3 or LAG3. (B) Scatter plots representing percentages of the four PD1/TIM3 and PD1/LAG3-expressing CD8^{+} TIL populations as described in (A). (C) SPICE analysis representing percent expression and co-expression of inhibitory receptors on CD8^{+} TILs of B16-tumor bearing *Foxp3*$^{\text{Cre-YFP}}$.*Ebi3*$^{\text{L/L}}$ mice and *Foxp3*$^{\text{Cre-YFP}}$ control mice. (D) Flow cytometric analysis depicting expression of inhibitory receptors (PD1/TIM3 and PD1/LAG3) on tumor-infiltrating CD4^{+}Foxp3^{-} T cells from B16 tumor-bearing *Foxp3*$^{\text{Cre-YFP}}$.*Ebi3*$^{\text{L/L}}$ mice and *Foxp3*$^{\text{Cre-YFP}}$ control mice. Cells gated on CD4^{+}Foxp3^{-} T cells, and assessed for percentages of PD1-high (PD1$^{\text{hi}}$), PD1-intermediate (PD1$^{\text{int}}$) and PD1-negative (PD1$^{\text{neg}}$)

fractions co-expressing TIM3 or LAG3. (E) Scatter plots representing percentages of the four PD1/TIM3 and PD1/LAG3-expressing $CD4^{+}Foxp3^{-}$ TIL populations as described in (D). (F) SPICE analysis representing percent expression and co-expression of inhibitory receptors on $CD4^{+}Foxp3^{-}$ TILs of B16-tumor bearing *Foxp3*$^{\text{Cre-YFP}}$.*Ebi3*$^{\text{L/L}}$ mice and *Foxp3*$^{\text{Cre-YFP}}$ control mice. Data represents 4 independent experiments; Error bars represent SEM; **, $p < 0.01$; ***, $p < 0.001$; ****, $p < 0.0001$; ns, non-significant (Unpaired Student's t-test). See also Figure S7.